



Supplementary information (Figs. S1–S9)

## **Single-cell and spatial transcriptomic analysis reveals that an immune cell-related signature could predict clinical outcomes for microsatellite-stable colorectal cancer patients receiving immunotherapy**

Shijin YUAN<sup>1,2</sup>, Yan XIA<sup>1,3</sup>, Guangwei DAI<sup>1,3</sup>, Shun RAO<sup>1,3</sup>, Rongrong HU<sup>1,3,4</sup>, Yuzhen GAO<sup>1,3</sup>, Qing QIU<sup>1,3</sup>, Chenghao WU<sup>1,3</sup>, Sai QIAO<sup>1,3</sup>, Yinghua XU<sup>2</sup>, Xinyou XIE<sup>1,3</sup>, Haizhou LOU<sup>2</sup>, Xian WANG<sup>2</sup>, Jun ZHANG<sup>1,3</sup>

<sup>1</sup>Department of Clinical Laboratory, Sir Run Run Shaw Hospital, Zhejiang University School of Medicine, Hangzhou 310016, China

<sup>2</sup>Department of Medical Oncology, Sir Run Run Shaw Hospital, Zhejiang University School of Medicine, Hangzhou 310016, China

<sup>3</sup>Key Laboratory of Precision Medicine in Diagnosis and Monitoring Research of Zhejiang Province, Hangzhou 310016, China

<sup>4</sup>Yongkang Hospital of Traditional Chinese Medicine Medical Community Xicheng Branch, Jinhua 321300, China

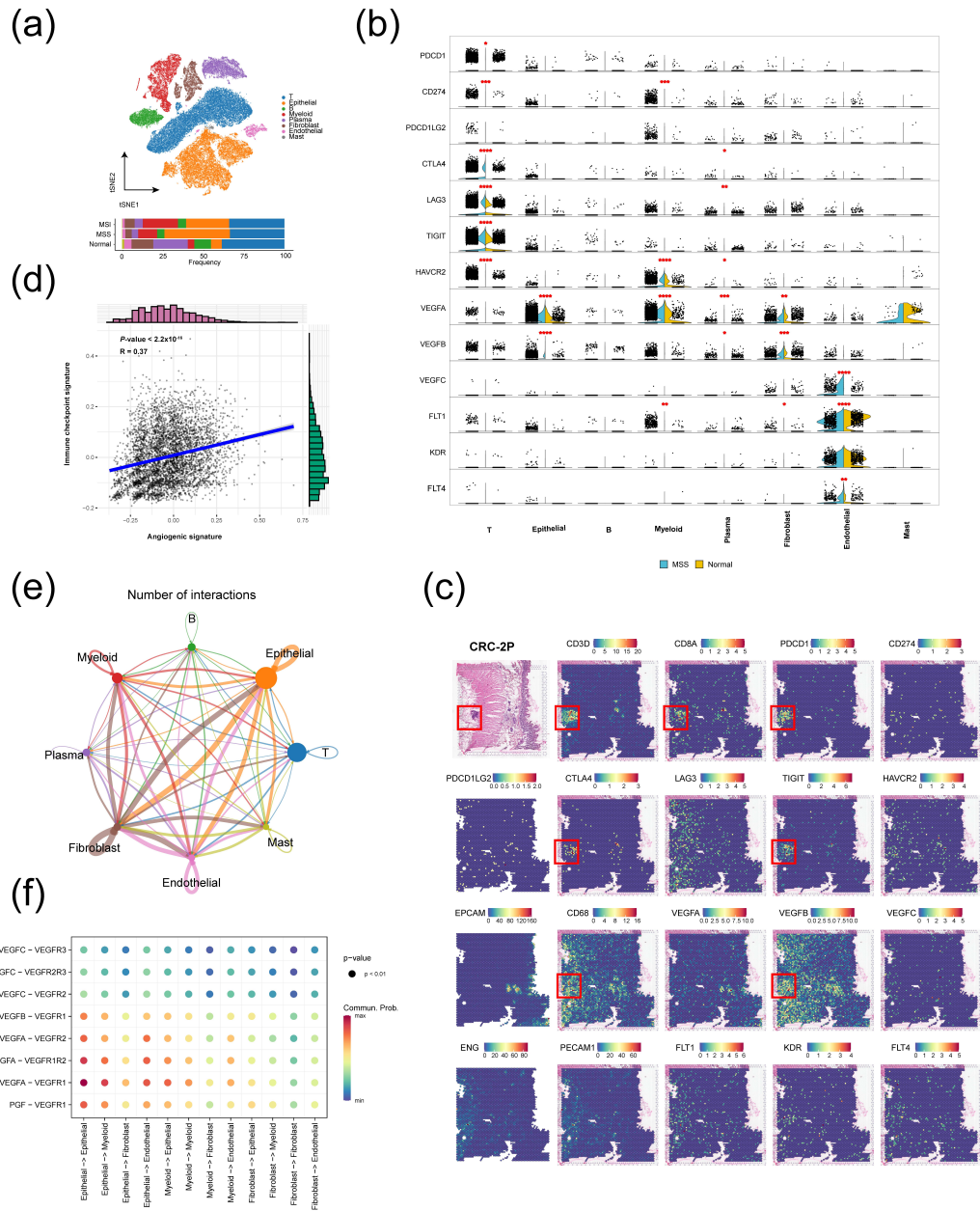


**Fig. S1 Immune and angiogenic landscape in MSS CRC tumor microenvironment**

**Fig. S1a** tSNE plot showing the annotation and color codes for TME cell types in CRC.

**Fig. S1b** Violin plots showing the expression of selected immune checkpoint and VEGF pathway-related genes between MSS tumor (blue) and normal tissue (yellow) (Wilcoxon test).

**Fig. S1c** The expression of immune checkpoint and VEGF pathway-related genes in spatial transcriptomic data from CRC patient.

**Fig. S1d** The Pearson correlation of signature score of immune checkpoint and angiogenesis in spatial transcriptomic data from CRC patient.

**Fig. S1e** Cell-cell communications of main CRC TME cell types by cell-chat analysis.

**Fig. S1f** Interaction analysis showing enriched VEGF pathway-related receptor-ligand pairs in main CRC TME cell types.

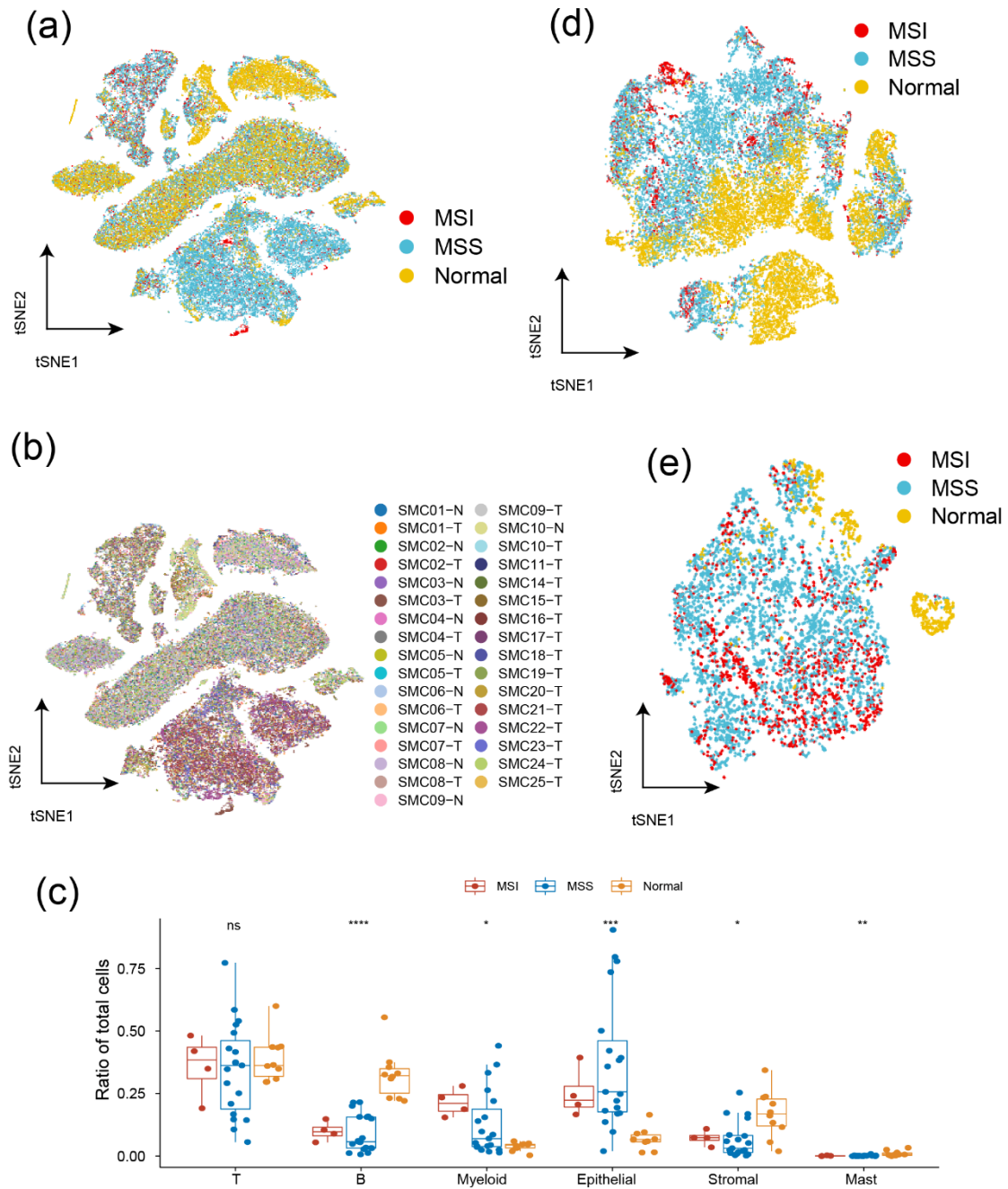


**Fig. S2 A single-cell transcriptomic atlas in MSS CRC tumor immune microenvironment**

**Fig. S2a, S2b** tSNE plot showing CRC TME cell origins by color, tissue origin **a)** and patient origin **b)**.

**Fig. S2c** Boxplot of CRC TME cell types fraction in MSI tumor (red), MSS tumor (blue) and normal tissue (green) (Kruskal-Wallis test).

**Fig. S2d** tSNE plot showing lymphoid-derived cell subtypes origins by color, tissue origin.

**Fig. S2e** tSNE plot showing myeloid-derived cell subtypes origins by color, tissue origin.

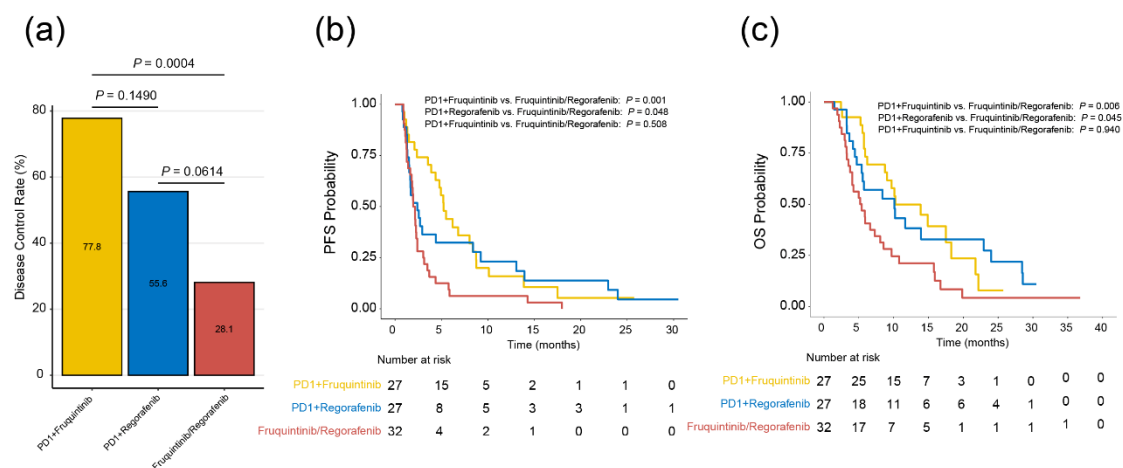


**Fig. S3 Immunotherapy combined with anti-angiogenic therapy improved the clinical outcomes of MSS CRC patients**

**Fig. S3a** Barplot showing the treatment response comparison among anti-PD-1 antibody plus fruquintinib, anti-PD-1 antibody plus regorafenib, and VEGFRi group (Chi-square test).

**Fig. S3b, S3c** Kaplan-Meier analysis of PFS **b)** and OS **c)** among anti-PD-1 antibody plus fruquintinib, anti-PD-1 antibody plus regorafenib, and VEGFRi group (log-rank test).



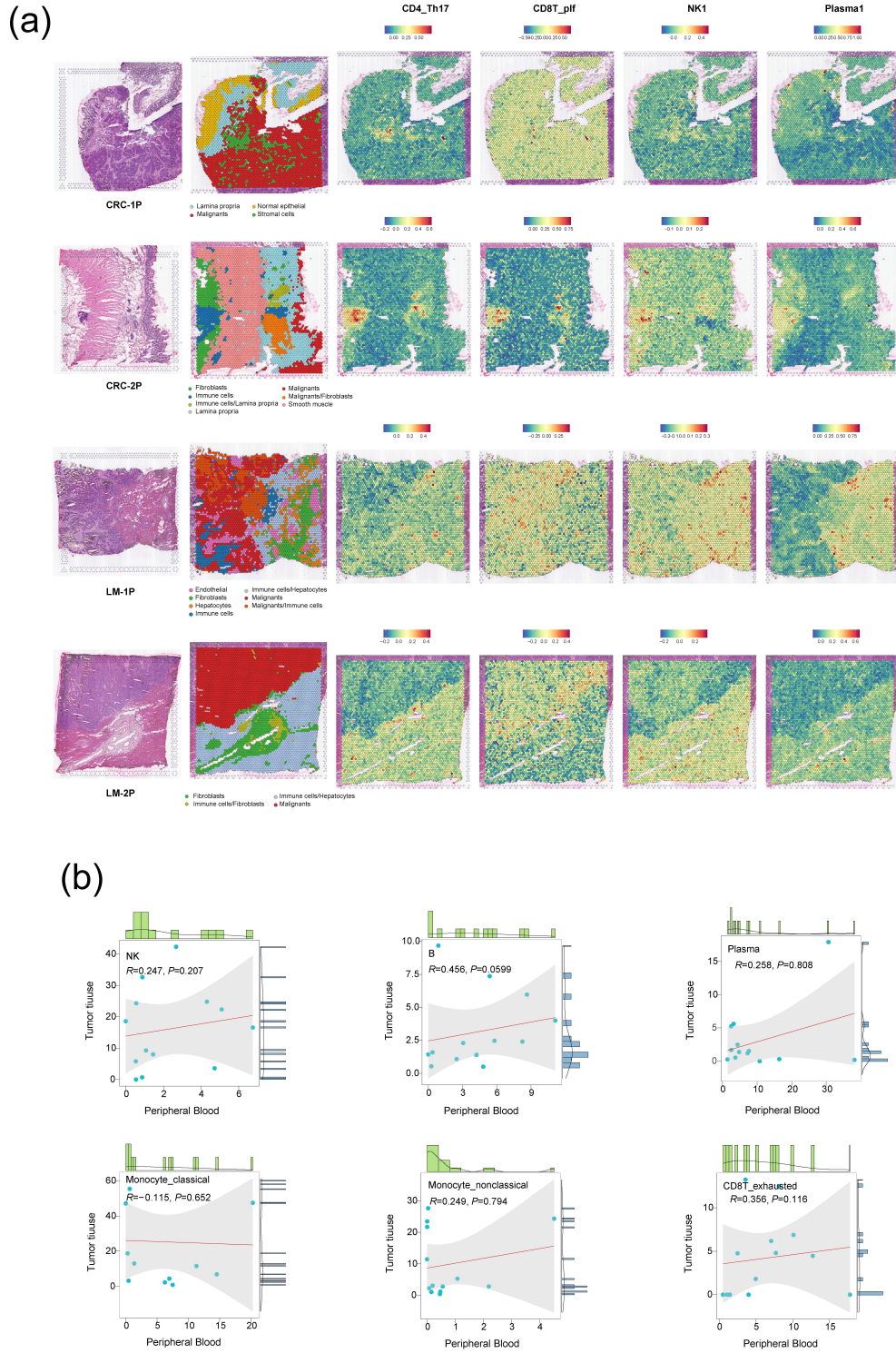


**Fig. S4 Spatial and peripheral blood single-cell transcriptomic landscape in MSS CRC**

**Fig. S4a** The H&E staining section, unsupervised clustering analysis and MSS CRC-enriched immune cell distribution of spatial transcriptomic data from CRC patients with primary tumor and liver metastasis.

**Fig. S4b** The Pearson correlation of MSS CRC-enriched immune cell type proportion from tumor and peripheral blood samples.

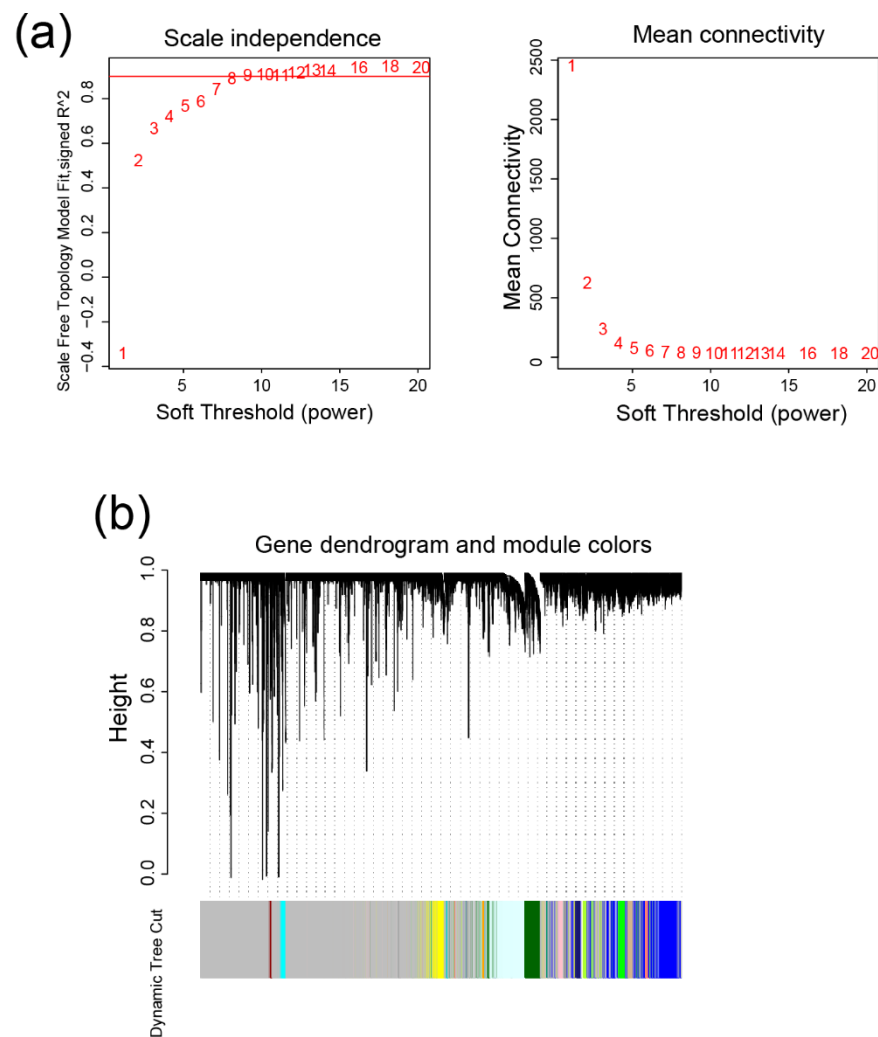


**Fig. S5 Identification of MSS CRC immune cell-related modules and hub genes**

**Fig. S5a** Analysis of network topology for different soft-threshold power. The left panel shows the impact of soft threshold power on the scale-free topology fit index; the right panel displays the impact of soft-threshold power on the mean connectivity.

**Fig. S5b** The gene dendrogram and module colors.

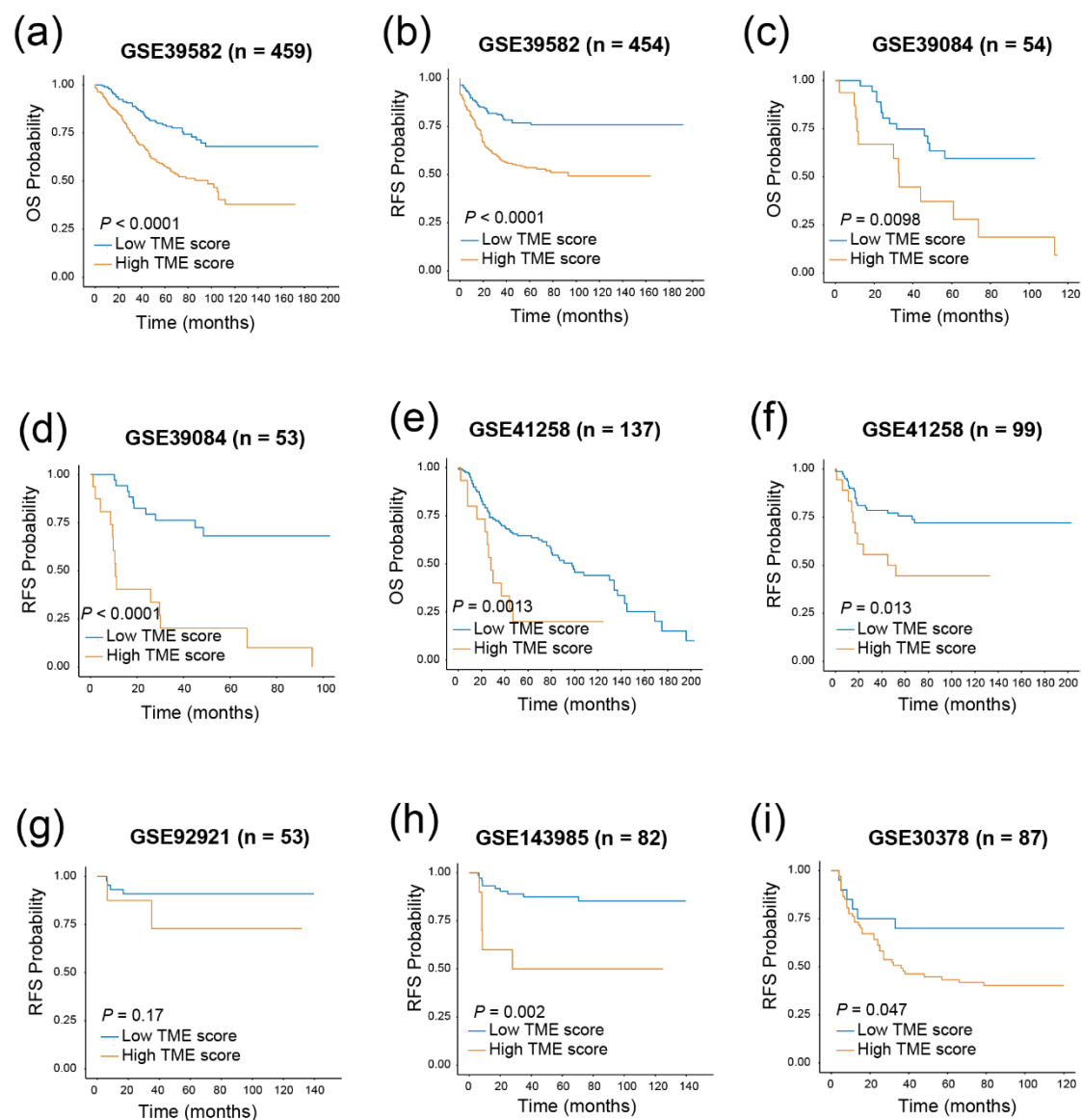


**Fig. S6 Construction of MSS CRC immune cell-related signature**

**Fig. S6a, S6b** The OS **a**) and RFS **b**) analysis according to MCICRS for GSE39582 cohort (log-rank test).

**Fig. S6c, S6d** The OS **c**) and RFS **d**) analysis according to MCICRS for GSE39084 cohort (log-rank test).

**Fig. S6e, S6f.** The OS **e**) and RFS **f**) analysis according to MCICRS for GSE41258 cohort (log-rank test).

**Fig. S6g-S6i** The RFS analysis according to MCICRS for GSE92921 cohort **g**), GSE143985 **h**) and GSE30378 **i**) cohort (log-rank test).

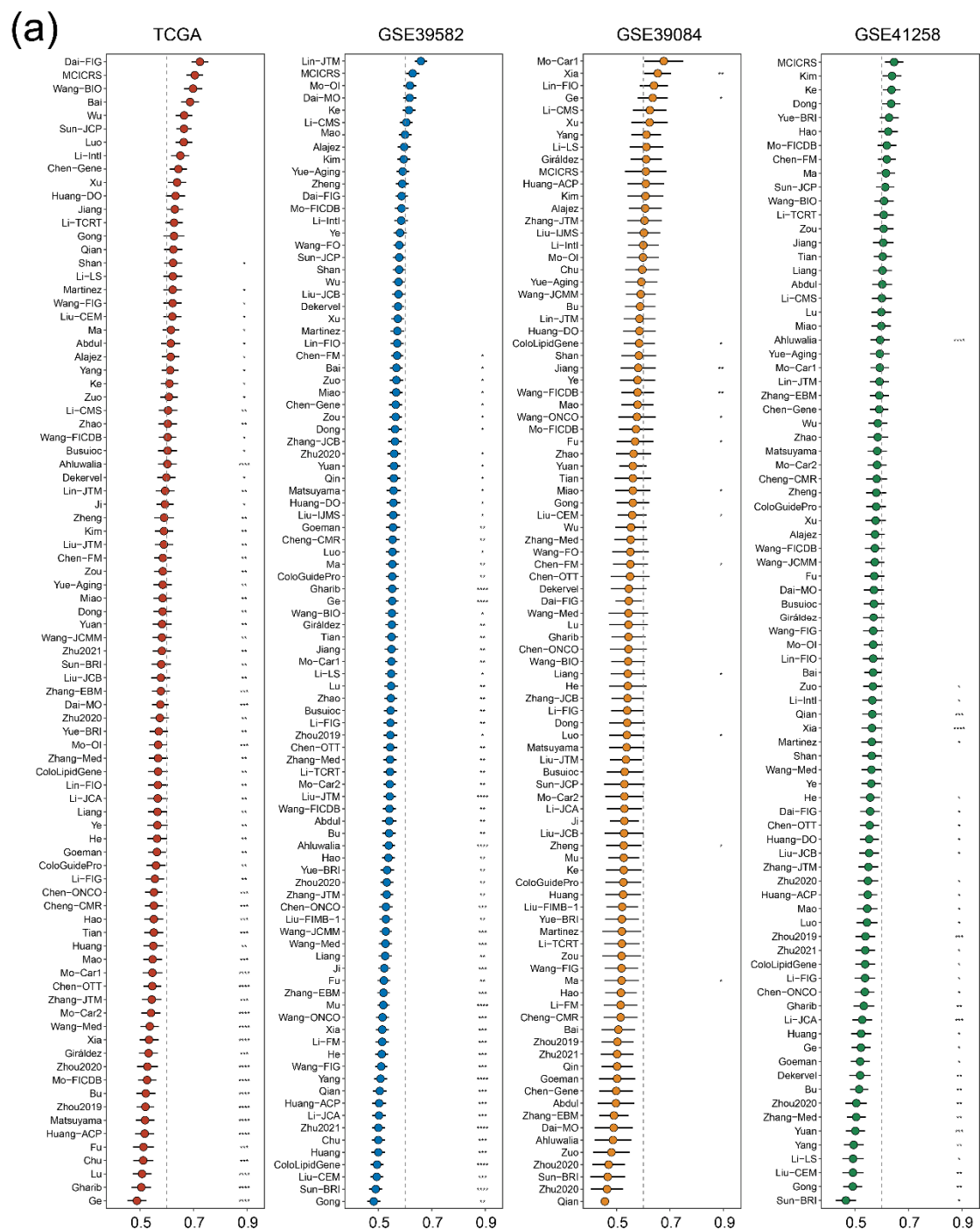


**Fig. S7 Comparison of gene expression-based prognostic signatures in CRC**

**Fig. S7a** Comparison of C-index among MCICRS and 104 published signatures in four cohorts.

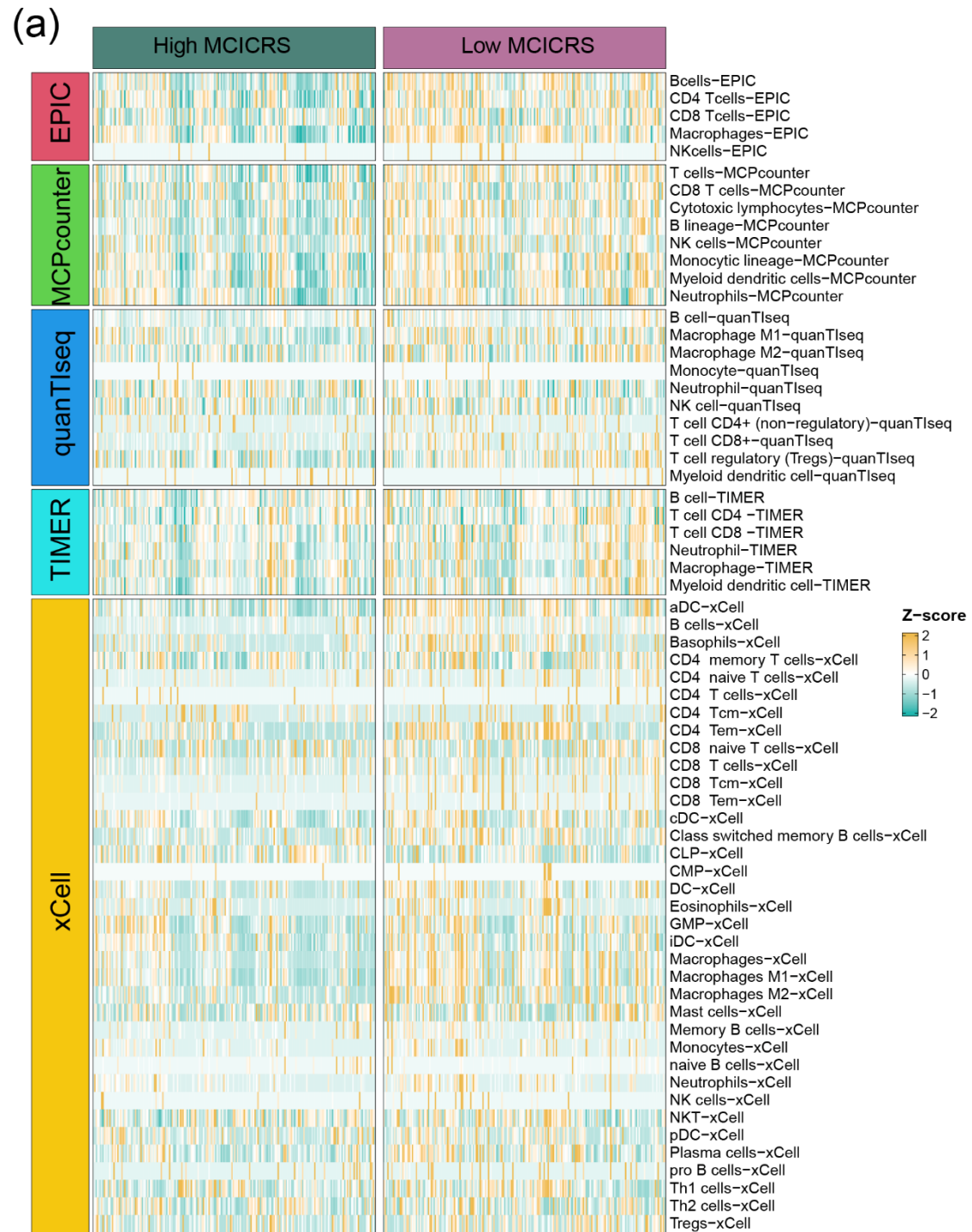


**Fig. S8 Immune infiltration characteristics of MCICRS**

**Fig. S8a** The infiltration abundance of different immune cell subsets evaluated by xCell, TIMER, quanTiseq, MCPcounter and EPIC algorithms for MCICRS-low and -high groups.



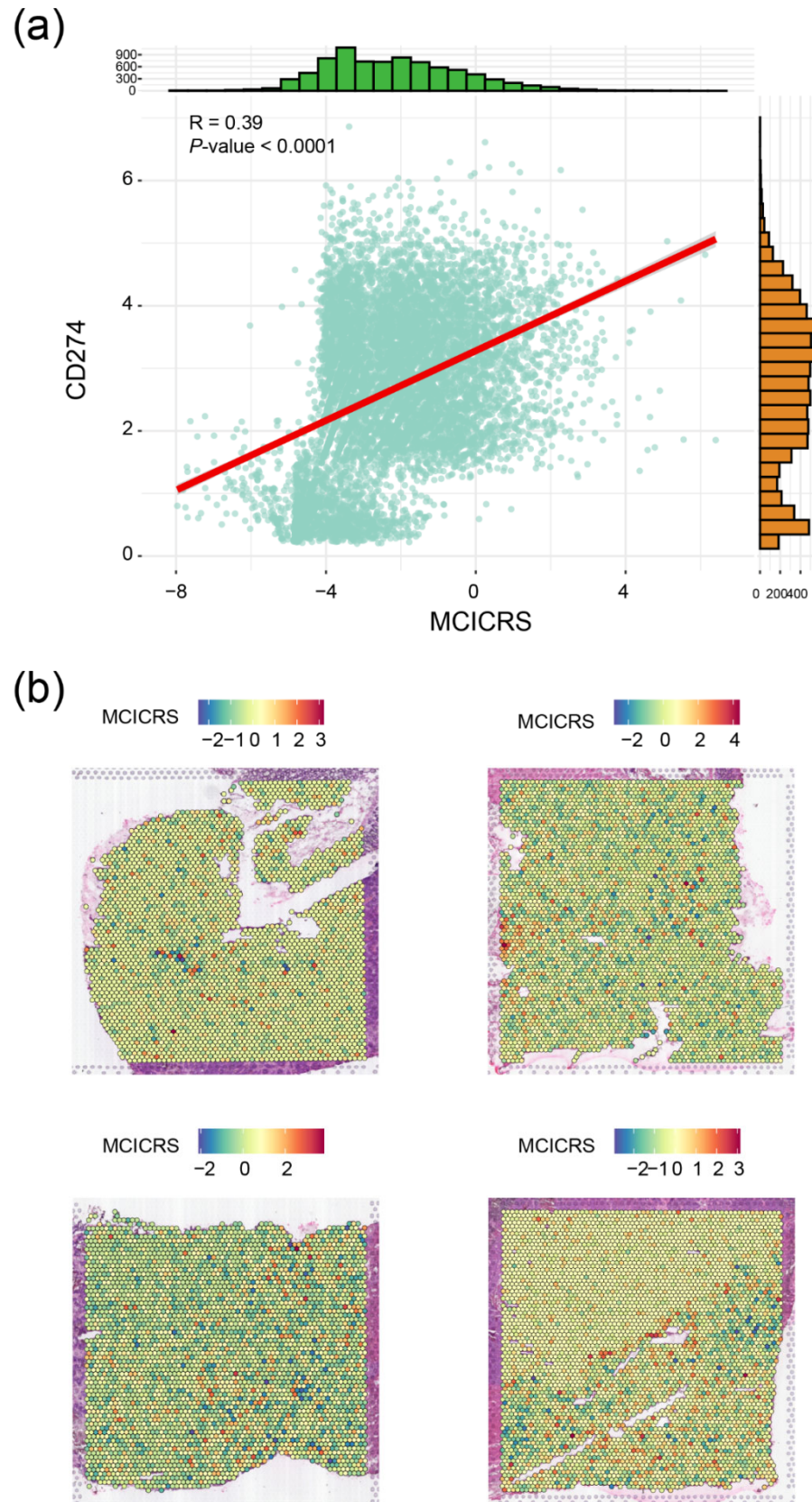


**Fig. S9 Immune and spatial characteristics of MCICRS**

**Fig. S9a** Scatterplots between MCICRS and *CD274* expression in CRC scRNA-seq data.

**Fig. S9b** The spatial distribution of MCICRS in ST data from CRC patients with primary tumor and liver metastasis.